

<https://doi.org/10.1038/s42005-025-02107-z>

Anomalously slow hot carrier cooling and insulator-to-metal transition in a photo-doped Mott insulator



Usama Choudhry¹, Jin Zhang^{2,3}✉, Kewen Huang⁴, Emma Low⁴, Yujie Quan¹, Basamat Shaheen¹, Ryan Gnabasi¹, Jiaqiang Yan⁵, Angel Rubio^{2,6,7}✉, Kenneth S. Burch⁴ & Bolin Liao¹✉

Photo-doped Mott insulators can exhibit novel photocarrier transport and relaxation dynamics and non-equilibrium phases. However, time-resolved real-space imaging of these processes are still lacking. Here, we use scanning ultrafast electron microscopy (SUEM) to directly visualize the spatial-temporal evolution of photoexcited species in a spin-orbit assisted Mott insulator α -RuCl₃. At low optical fluences, we observe extremely long hot photocarrier transport time over one nanosecond, almost an order of magnitude longer than any known values in conventional semiconductors. At higher optical fluences, we observe nonlinear features suggesting a photo-induced insulator-to-metal transition, which is unusual in a large-gap Mott insulator. Our results demonstrate the rich physics in a photo-doped Mott insulator that can be extracted from spatial-temporal imaging and showcase the capability of SUEM to sensitively probe photoexcitations in strongly correlated electron systems.

Understanding and tuning the complex coupling behaviors among charge, spin, orbital, and lattice degrees of freedom in strongly correlated electronic systems has been a central theme in condensed matter physics¹. As an important example, Mott insulators are insulating phases created by strong electron-electron repulsions in materials that should be metallic based on the non-interacting electron band theory². In a Mott insulator, the onsite Coulombic repulsion between electrons overcomes the tendency of the electronic wave functions to spread and minimize their kinetic energy, leading to localized electrons and an insulating state. The close interplay between competing energy scales in Mott insulators can lead to collective behaviors, causing large variations in physical properties in response to small perturbations. As a result, perturbing the ground state of a Mott insulator, e.g. by doping, changing temperature and pressure, applying external electrical and magnetic fields, and photoexcitation, can lead to a gamut of exotic phenomena of both fundamental interest and technological relevance, such as high-temperature superconductivity³, metal-insulator transitions⁴, and colossal magnetoresistance⁵. Despite extensive research efforts, the microscopic details of these processes remain to be understood.

Among various external perturbations, optical excitation provides a precise way to introduce mobile charges into Mott insulators and monitor

their subsequent response with high temporal resolution enabled by ultrafast lasers⁶. In addition, a large Mott gap can reduce trivial laser heating and suppress thermalization of hot photocarriers, which can give rise to novel nonequilibrium states⁶. For these reasons, a range of optical pump-probe methods, including transient optical spectroscopy, time-resolved photoemission spectroscopy, and time-resolved X-ray spectroscopy, have been applied to investigate the dynamics of photoexcited carriers and, more interestingly, photo-induced nonequilibrium phases in Mott insulators^{7,8}. However, these existing studies based on optical spectroscopy and diffraction lack the spatial resolution to visualize the spatial-temporal evolution of photoexcited states, which, crucially, can reveal the impact of correlation on transient transport properties in Mott insulators. Scanning ultrafast electron microscopy (SUEM) is an emerging technique that can image the spatial-temporal evolution of surface photocarrier dynamics. SUEM is a photon-pump-electron-probe technique that uses short electron pulses with picosecond duration to image the response of a sample surface after the impact of a photon pulse^{9,10}. It integrates the temporal resolution of femtosecond lasers with the spatial resolution of scanning electron microscopes (SEMs). The change of local secondary electron (SE) yield as a result of the optical excitation is measured and used to form difference images¹¹. Given the

¹Department of Mechanical Engineering, University of California, Santa Barbara, CA, USA. ²Max Planck Institute for the Structure and Dynamics of Matter and Center for Free-Electron Laser Science, Hamburg, Germany. ³Laboratory of Theoretical and Computational Nanoscience, National Center for Nanoscience and Technology, Chinese Academy of Sciences, Beijing, China. ⁴Department of Physics, Boston College, Chestnut Hill, MA, USA. ⁵Materials Science and Technology Division, Oak Ridge National Laboratory, Oak Ridge, TN, USA. ⁶Center for Computational Quantum Physics, The Flatiron Institute, New York, NY, USA. ⁷Nano-Bio Spectroscopy Group, Universidad de País Vasco, San Sebastián, Spain. ✉e-mail: jinzhang@nanocr.cn; angel.rubio@mpsd.mpg.de; bliao@ucsb.edu

shallow escape depth of SEs (a few nanometers), SUEM is highly sensitive to surface charge dynamics and has been used to study photocarrier diffusion in uniform semiconductors^{12,13} and near interfaces^{9,14}. So far, SUEM has only been applied to image photocarrier dynamics in conventional semiconductors without strong electron correlation effects.

In this work, we report time-resolved imaging of photoexcited states in a van der Waals layered Mott insulator α -RuCl₃ with SUEM. α -RuCl₃ is a 4d-transition-metal halide composed of honeycomb layers made of adjoining RuCl₆ octahedra¹⁵. Comprehensive photoemission, optical, magnetic, and transport measurements have suggested that it is a spin-orbit assisted Mott insulator with a wide Mott gap¹⁶, which is a result of both strong electron correlations and spin-orbit coupling¹⁵. The combination of a Mott insulating state and a honeycomb lattice of strongly spin-orbit-coupled transition metal ions has been identified as a potential ingredient for actualizing Kitaev quantum spin liquids^{17,18}, leading to extensive studies of α -RuCl₃ in pursuit of these states^{19,20}. In addition, theoretical studies have predicted that the Mott insulating state in α -RuCl₃ can be sensitively tuned by photoexcitation, leading to optically driven magnetic^{21,22} and insulator-to-metal²³ transitions. These rich physics make α -RuCl₃ a particularly interesting material to study with SUEM. Here, we use SUEM to image the spatial-temporal evolution of photoexcited states in α -RuCl₃ across different optical excitation fluences. At low optical fluences, we observe diffusion of photoexcited species with an extremely long hot carrier transport time beyond 1 ns at room temperature, which is almost one order of magnitude longer than known values in a conventional semiconductor¹². At higher optical fluences, we observe nonlinear responses suggesting a photo-induced insulator-to-metal transition with an onset at as low as roughly 0.01 photoexcited electrons per unit cell. Our result suggests the electronic structure in α -RuCl₃ can be sensitively controlled by a low concentration of photoexcited carriers at room temperature and showcases the capability of SUEM to probe spatial-temporal dynamics of photo-doped strongly correlated electronic systems.

Results and discussion

Details of our SUEM setup are described elsewhere¹² and can be found in the “Methods” section and Figs. S1 and S2 in the Supplementary Information. Briefly, we use an optical pump pulse [wavelength: 515 nm (2.4 eV), pulse duration: 150 fs, repetition rate: 5 MHz, beam diameter 30 μ m] to excite the sample and use a delayed electron-probe pulse (“primary electrons”, or PEs; 25 electrons per pulse, energy: 30 keV). The electron pulses are generated by illuminating a Schottky electron gun with ultraviolet optical pulses (wavelength: 257 nm) from the same laser source. Upon impact of the PEs on the sample surface, SEs emitted from each location on the sample surface are collected by an Everhart-Thornley detector. The change of local SE yield as a result of the optical excitation, which is sensitive to the average electron energy, potential, and conductivity near the sample surface¹⁷, is used to form SUEM difference images. The spatial resolution of these images is on the order of the size of the PE beam (a few nanometers), and the time resolution is determined by the duration of the PE pulses, which broadens from 150 fs to a few picoseconds when using around 100 electrons per pulse due to space-charge effects^{12,24}. All experiments are conducted at room temperature with a vacuum level of 8×10^{-7} torr.

α -RuCl₃ crystals are exfoliated onto Si/SiO₂ substrates in a glovebox to minimize water exposure that can easily intercalate it²⁵. More details can be found in the “Methods” section. Optical and electrical characterizations of our α -RuCl₃ samples have been reported in a previous publication²⁵. Figure 1a shows representative SUEM images taken on a α -RuCl₃ flake on an Si/SiO₂ substrate using an optical pump fluence of 30 μ J cm⁻². Each difference image is obtained by subtracting a reference image that is taken at a far negative time, and thus, the contrast in the images is representative of the change in SE emission from the sample surface because of photoexcitation. The lack of contrast at -60 ps indicates that the 200 ns interval between pump pulses is sufficiently long to allow the sample to equilibrate between pumping events. After time zero, a bright contrast emerges from the pump-illuminated region, indicating that SE emission from the area has increased.

As established in SUEM, this contrast correlates with the distribution of carriers near the sample surface and results from the increased average energy of local electrons due to photoexcited carriers¹¹.

In the low fluence SUEM images shown in Fig. 1a, the evolution of the contrast suggests a diffusion process of a photoexcited species on the timescale of hundreds of picoseconds to a few nanoseconds. The diffusion process can be quantified by fitting the SUEM contrast to a two-dimensional Gaussian function with time-dependent magnitude and radius¹² (see Supplementary Note 1 for more information). The fitted time-dependent magnitude is shown in Fig. 1b, suggesting a recombination lifetime of 2.3 ± 0.3 ns. The fitted time-dependent radius is shown in Fig. 1c. The diffusivity of the photocarriers depends on time, due to the “hot” state of the photocarriers immediately after excitation, since the pump energy (2.4 eV) is much higher than the optical gap of 1 eV in α -RuCl₃¹⁵. The diffusivity decays as the hot photocarriers thermalize and cool down to the band edges through interactions with phonons and spins. Hot photocarrier transport has been observed with SUEM in a range of conventional semiconductors^{10,12,26}, which can persist for over 200 ps in boron arsenide due to a hot phonon bottleneck effect¹². The hot photocarrier diffusion behavior can be quantified by analyzing the SUEM contrast using a diffusion equation with an exponentially decaying diffusivity with a time constant τ , $D(t) = (D_i - D_0)e^{-t/\tau} + D_0$, where D_i is the effective diffusivity immediately after photoexcitation, and D_0 is the equilibrium diffusivity at 300 K. The fitting is shown in Fig. 1c for an optical fluence of 30 and 40 μ J cm⁻², where an extremely long hot carrier transport time τ of roughly 1 ns at 30 μ J cm⁻² (1.5 ns at 40 μ J cm⁻²) and an initial diffusivity of 2000 cm² s⁻¹ are extracted. The initial diffusivity is orders of magnitude lower than that in silicon²⁶. Our low fluence result suggests that the hot photocarriers in α -RuCl₃ diffuse more slowly than those in conventional semiconductors but cool down to the band edges on a much longer timescale (almost one order of magnitude longer than that in boron arsenide).

We observe qualitatively different SUEM contrasts at increased optical pump fluences. Figure 2a shows representative SUEM difference images using a fluence of 400 μ J cm⁻². This fluence corresponds to roughly 0.02 photoexcited electrons per unit cell near the center of the Gaussian pulse (see Supplementary Note 2 for more discussions). No contrast is visible at negative times, once again indicating that the sample is adequately relaxed between pump events. After a few ps, instead of observing a Gaussian region of bright contrast, a ring of bright contrast is present with a central area of dark contrast. The area of bright contrast expands slightly over a few hundred picoseconds before relaxing on a timescale roughly similar to the low fluence measurements. However, the region of dark contrast persists for the full 4 nanoseconds that are accessible to the experiment. Additional SUEM image series are shown in the Supplementary Information (Figs. S3–S13) for intermediate fluences between 10 and 400 μ J cm⁻².

While there is some deviation in the observed image contrast due to variation in absorption between different locations on the different samples, two general observations can be made: (1) the overall contrast magnitude is observed to decrease with increasing pump fluence, which is in sharp contrast to all previous SUEM studies, and (2) the magnitude of the dip in the center of the pump-illuminated region increases with fluence. Therefore, at intermediate fluences between 30 and 400 μ J cm⁻², this feature begins to manifest first as a small decrease in contrast while remaining positive in magnitude. At higher fluences, the center region becomes dark, indicating that SE emission is suppressed in the region of the sample experiencing the greatest instantaneous fluence. These features can be seen clearly in Fig. 2b, c, where line cuts of the SUEM contrasts at different optical fluences are shown. A systematic examination of the SUEM images taken at different optical fluences is shown in Fig. S3, which indicates an onset of the nonlinear feature at a fluence around 40 μ J cm⁻², although variation of this critical fluence between different locations of different samples is observed. We also carefully design the order of measurements with different optical fluences to rule out the potential trivial explanation that the observed contrast is due to some laser-induced damage of the samples (see Fig. S4).

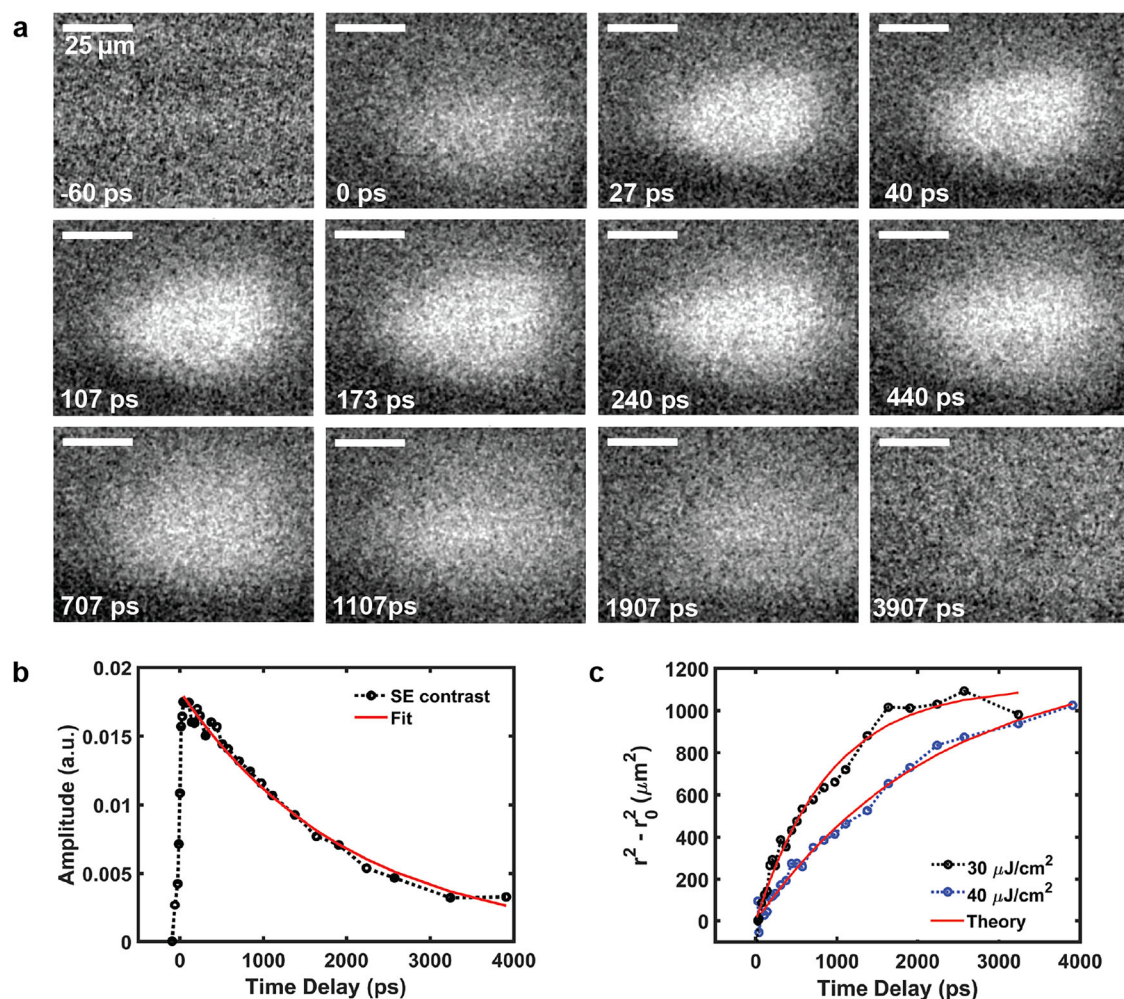


Fig. 1 | Scanning ultrafast electron microscopy (SUEM) difference images of α - RuCl_3 taken at low optical fluences. **a** SUEM difference images taken as a function of delay time with an optical pump fluence of $30 \mu\text{J}/\text{cm}^2$. The bright contrast indicates enhanced secondary electron yield in the photoexcited region. **b** Amplitude of the SUEM contrast (fitted to two-dimensional Gaussian functions) as a function of

delay time with an optical pump fluence of $30 \mu\text{J}/\text{cm}^2$, suggesting a photocarrier recombination lifetime of 2.2 ns. **c** Radius of the SUEM contrast (fitted to two-dimensional Gaussian functions; original radius r_0 subtracted) as a function of delay time at optical fluences of 30 and $40 \mu\text{J}/\text{cm}^2$. The theoretical model used to fit the data is explained in the Supplementary Note 1.

Figure 3a, b summarizes the evolution of the magnitude of the SUEM contrast in different regions of interest spanning fluences from 50 to $400 \mu\text{J}/\text{cm}^2$. Figure 3a shows the change in contrast for the center region, while Fig. 3b tracks the brightest region on the shoulder of the pump spot. As observed, the signal level in the center of the pump spot is lower than that on the edge, and the overall signal level decreases as the pumping fluence increases. Figure 3c, d shows the normalized change in contrast in order to better compare changes in relaxation at different fluences. Figure 3c indicates that there is no obvious change in relaxation dynamics in the center region at low fluences, but at high fluences, the behavior becomes obviously different. At $250 \mu\text{J}/\text{cm}^2$, the contrast in the center decays quicker than at lower fluences, while at 300 and $400 \mu\text{J}/\text{cm}^2$, the contrast becomes persistently negative. The transition starts to occur around $200 \mu\text{J}/\text{cm}^2$, which corresponds to roughly 0.01 electrons photoexcited per unit cell near the center of the pump beam. Curiously, the contrast on the bright edge of the pump spot (Fig. 3d) does not show any change in relaxation dynamics as a function of fluence, with a recombination lifetime of roughly 2.5 ns across all fluences. Representative difference images showing these behaviors are provided in Fig. S5 of the Supplementary Information.

In Mott insulators, excited carriers can be described as negative doublons, corresponding to doubly occupied sites, and positive holons, corresponding to unoccupied sites. There are theoretical predictions that the relaxation time scales for doublons and holons in Mott insulators increase

rapidly when the onsite Coulomb energy U becomes much larger than the bandwidth due to a thermalization bottleneck^{27,28}, which can potentially explain the long relaxation lifetime we observe at low optical fluences. However, the extremely long hot photocarrier transport time over 1 ns has not been observed in a Mott insulator. Doublons and holons can also form Mott-Hubbard excitons (MHEs), which were proposed to explain time-resolved two-photon photoemission spectroscopy and transient reflection spectroscopy measurements on α - RuCl_3 ²⁹. The long hot photocarrier transport time observed in our experiment is similar to a slow timescale measured in their experiment²⁹, which was interpreted as the MHE lifetime. A potential explanation for the persistent hot photocarrier transport can be a cooling bottleneck between bands with different pseudospins $J_{\text{eff}} = 1/2$ and $J_{\text{eff}} = 3/2$ in α - RuCl_3 ^{30,31}, which is a unique feature in spin-orbit assisted Mott insulators.

The high-fluence SUEM features can be explained by a photo-induced insulator-to-metal transition³². SE yield sensitively depends on the local electrical conductivity³³, thus making SUEM a suitable tool to detect significant photo-induced conductivity changes. In an insulating material, slight charging of the sample due to primary electron injection can lead to surface electrostatic fields that enhance the SE yield. A photo-induced metallic state will suppress this electrostatic field and lead to a reduced SE yield. This effect can explain the reduced overall SUEM contrast at increased optical fluences, which is distinct from previous SUEM experiments.

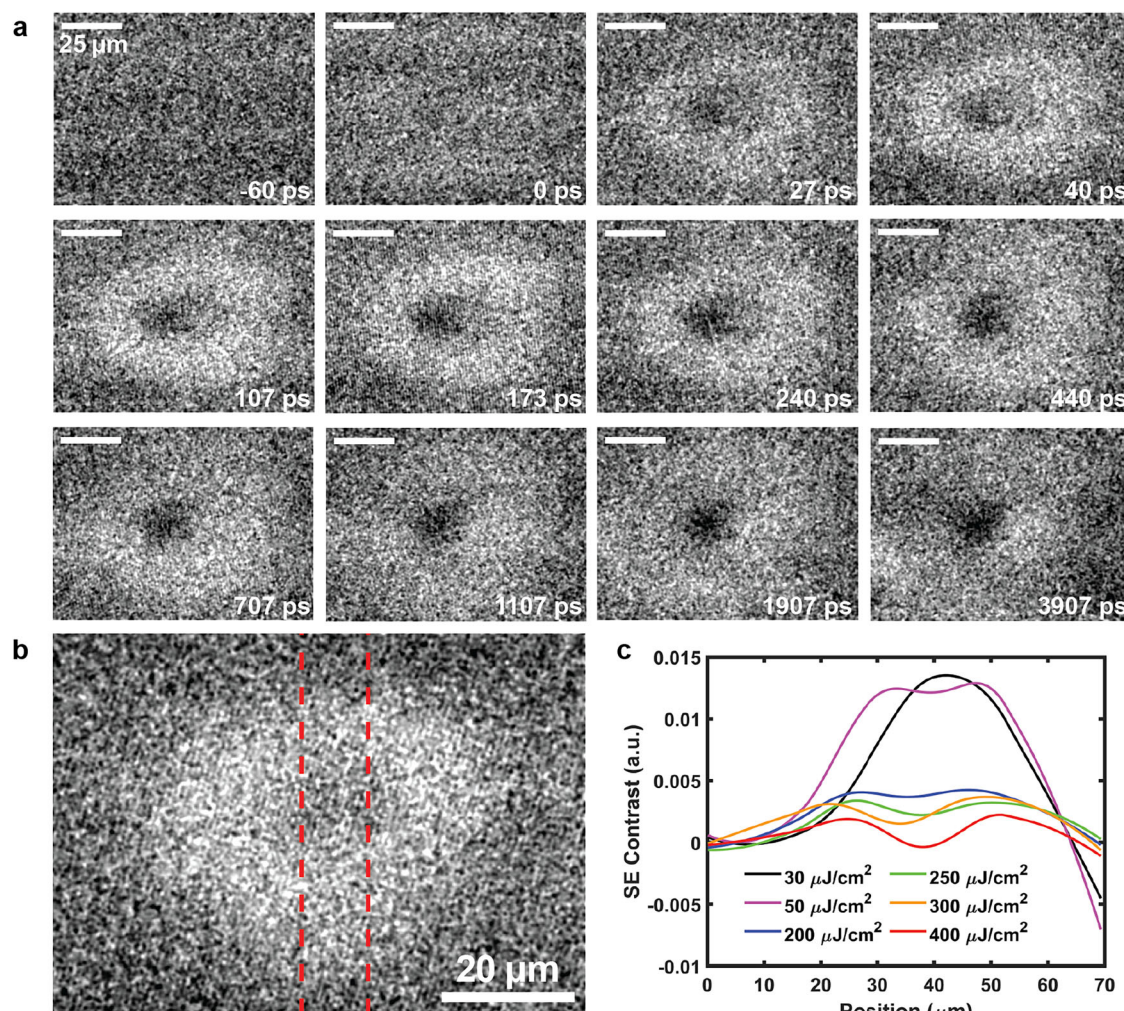


Fig. 2 | Scanning ultrafast electron microscopy (SUEM) difference images of α -RuCl₃ taken at high optical fluences. a SUEM difference images taken as a function of delay time with an optical pump fluence of 400 $\mu\text{J}/\text{cm}^2$. Highly nonlinear features including a center dark region and a bright outer region emerge at higher optical

fluences. **b** Representative SUEM image with red dashed lines indicating the regions of interest, where the line cuts shown in (c) are taken. **c** Line cuts of the SUEM contrast magnitude at different optical fluences, showing a reduced contrast in the center and overall suppressed contrast as the optical pump fluence is increased.

Furthermore, insulators typically have higher SE yield due to reduced electron-electron scatterings experienced by the SEs as they migrate through the sample before escaping from the surface³³. Thus, the photo-induced metallic conductivity can reduce the local SE yield, which competes with the more common effect that an increased average local electron energy due to photoexcitation enhances the SE yield. This trend is summarized in Fig. 4a. In the center of the Gaussian optical pump beam, the excitation level is the highest, which leads to the most suppressed SE yield, which manifests as a central dip or dark region in the SUEM images.

In a previous work²³, we have theoretically explored the possibility of a photo-induced insulator-to-metal transition in α -RuCl₃ using ab initio time-dependent density functional theory (TDDFT) with the ACBN0 functional developed to simulate electronic properties of strongly correlated materials³⁴. We found that above-gap photoexcitation significantly reduces the onsite energy U , which can lead to a melting of the Mott gap and an insulator-to-metal transition in α -RuCl₃ on a subpicosecond timescale. To better match the current experimental condition, we repeat the TDDFT simulation with 2.4 eV photon energy. Since it is computationally infeasible to match the experimental timescale using TDDFT, we simulate a short optical pulse (40 fs duration) instead, as shown in Fig. 4b, and track the dynamic evolution of the electronic band structure within 80 fs, which is much shorter compared to the experimental timescale. To compare to our experimental excitation level, we analyze the excited carrier density by

projecting the time-evolved wave functions on the ground state wave functions of α -RuCl₃²³. Under this condition, we observe that the melting of the Mott gap (the ground state and excited state electronic structures are shown in Fig. 4c, d, respectively) occurs when the photoexcited carrier concentration exceeds about 0.1 electron per unit cell in a similar manner as reported previously²³, which is one order of magnitude higher than the experimentally observed threshold. However, we caution that a direct comparison between the TDDFT simulation and our experimental observation in this work cannot be made reliably due to the significantly different time scales involved. Nevertheless, the TDDFT study points to photo-induced band structure renormalization as a possible mechanism for our observed insulator-to-metal transition. While photo-induced metallic states have been observed in small-gap Mott insulators^{35–37}, their realization in a large-gap Mott insulator such as α -RuCl₃ at a low excitation level is quite unusual, and more studies are required to clarify their nature.

In summary, our SUEM images in α -RuCl₃ suggest an anomalously long hot photocarrier transport time at low optical fluences, likely due to a cooling bottleneck between bands with different pseudospins, and a photo-induced insulator-to-metal transition at higher optical fluences. Both findings indicate interesting transport and relaxation mechanisms in photo-doped Mott insulators. These results also demonstrate SUEM as a sensitive probe to photo-induced nonequilibrium phases in strongly correlated electron systems.

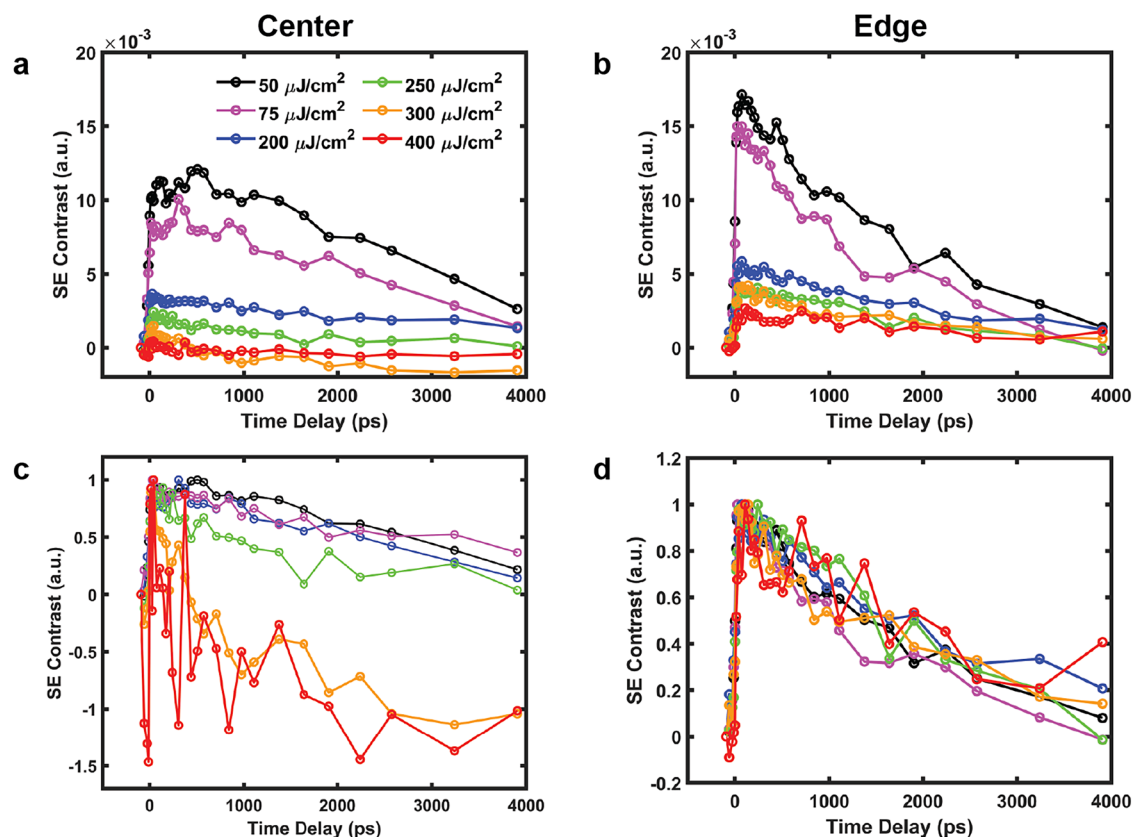


Fig. 3 | Evolution of the scanning ultrafast electron microscopy (SUEM) contrasts at high optical fluences. The evolution of the SUEM contrast in the center dark region and the outer bright region at different optical pump fluences is shown in (a) and (b). Normalized versions are shown in (c) and (d). While the relaxation

dynamics in the outer bright region are independent of the optical pump fluence, a sharp transition near $250 \mu\text{J}/\text{cm}^2$ is observed in the center region, signaling a photo-induced insulator-to-metal transition. Significant noise at higher optical fluences is due to reduced overall SUEM contrast.

Methods

Scanning ultrafast electron microscopy

This section provides a detailed description on the SUEM setup employed in this work (Figs. S1 and S2). A fundamental infrared (IR) laser pulse train (Clark MXR IMPULSE, wavelength: 1030 nm, pulse duration: 150 fs, repetition rate: 5 MHz) is directed to frequency-doubling crystals to create the visible pump beam (wavelength: 515 nm with tunable power) and the ultraviolet (UV) photoelectron excitation beam (wavelength: 257 nm, power: 15 mW). The visible pump beam travels variable distances adjusted by a mechanical delay stage (Newport DL600, delay time range: -0.7 ns to 3.3 ns). The UV excitation beam is directed through a transparent window on the column of an SEM (ThermoFisher Quanta 650 FEG) and onto the apex of a cooled Schottky field emission gun (a zirconium-oxide-coated tungsten tip), generating electron pulses with subpicosecond durations via the photoelectric effect. An electron current of 20 pA is used in this experiment, corresponding to 25 electrons per pulse. A time resolution of 2 ps is expected for 25 electrons per pulse. The photo-generated electron pulses are accelerated inside the SEM column to 30 keV kinetic energy, and are finely focused to a nanometer size through the electron optics in the SEM. The beam dwell time at each pixel was 300 ns. Each SUEM contrast image at a given delay time represented an average of 2000–4000 images. During the measurements, the photocathode was refreshed every 60 min to prevent the fluctuation of the cathode work function. A mechanical coupling system is built to make a rigid connection between the SEM air-suspension system and the optical table hosting the laser and the alignment system to minimize the relative vibration that affects the alignment at the photocathode.

Sample preparation

α -RuCl₃ single crystals used in this study were grown by a self-selecting vapor transport technique reported elsewhere³⁸. α -RuCl₃ flakes were then exfoliated from a bulk single crystal using Nitto tape. Flakes used in this study have a thickness ranging from 1 to 3 μm , which is much larger than the optical penetration depth, to avoid the interference from the substrate. These flakes were exfoliated onto n-doped Si/SiO₂ chips that were first cleaned by sonication in acetone for 10 min, then rinsed with IPA, and then de-ionized H₂O. These chips had been treated previously with photoresist in order to create markers on their surface for easy location in the SEM. The photoresist was removed during this cleaning process. The water was blown off with an argon gas gun, and the chip was baked for 5 min at 105 °C to remove any residual water on the surface. The samples were then searched using a microscope, and the surfaces of each flake were examined using dark field microscopy for a 1-s exposure time to see if there were any visible debris or defects on the flake's surface. The flakes were then characterized by Raman spectroscopy using 200 μW laser power. The single spectra were taken with 1800 grating per mm for 180. All studied flakes revealed Raman spectra consistent with bulk.

Theoretical simulations

The electronic properties of α -RuCl₃ are computed by the generalized Kohn–Sham equations within time-dependent density functional theory, including mean-field interactions, as provided by the Octopus package^{39,40}, using the ACBN0 functional together with the local density approximation (LDA) functional for describing the semi-local DFT part^{34,41}. To ensure accuracy, we incorporated experimental lattice parameters (specifically, 5.98 Å and 10.35 Å) and atomic positions³¹. Our computational setup features a mixed periodic boundary condition, including a 15 Å vacuum region

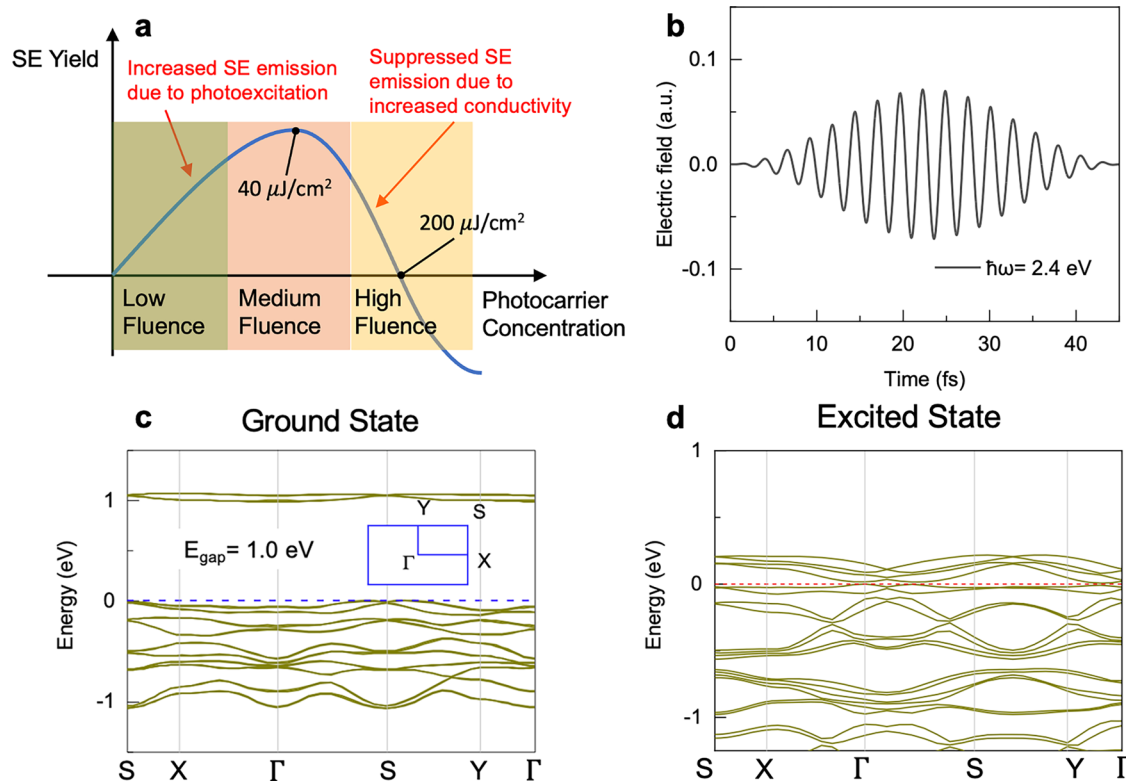


Fig. 4 | Physical picture of photo-induced scanning ultrafast electron microscopy (SUEM) contrast in α -RuCl₃. **a** Schematic showing the competing mechanisms affecting the secondary electron (SE) yield as a function of photocarrier concentration. At low optical fluences, increased average electron energy due to photoexcitation enhances the SE yield. At higher optical fluences, increased local conductivity due to photo-induced insulator-to-metal transition suppresses the SE yield. **b** The electric field profile used in the time-dependent density functional

theory (TDDFT) simulation as the optical excitation. **c** The ground state electronic structure calculated using the density functional theory (DFT) with the ACBN0 functional, showing an optical gap of 1 eV. The inset shows the first Brillouin zone and the high-symmetry points. **d** The electronic structure at 80 fs after photo-excitation simulated using TDDFT with an excitation level of 0.1 electron per unit cell, showing a complete melting of the Mott gap.

to minimize interactions between periodic images. We employed norm-conserving HGH pseudopotentials⁴², maintained a real-space grid spacing of 0.33 atomic units, and employed an $8 \times 6 \times 1$ k-point grid within a $1 \times \sqrt{3}$ supercell with a rhombus shape, accommodating 16 atoms for the zigzag antiferromagnetic order. Spin-orbit coupling is a critical factor in deriving the correct electronic and magnetic structures in α -RuCl₃. Converged effective Hubbard U terms were determined with the ACBN0 functional, resulting in values of 1.96 eV for Ru 4d orbitals and 5.31 eV for Cl 3p orbitals, respectively.

Data availability

Data sets generated during the current study are available from the corresponding author on reasonable request.

Received: 26 February 2025; Accepted: 22 April 2025;

Published online: 02 May 2025

References

- Dagotto, E. Complexity in strongly correlated electronic systems. *Science* **309**, 257–262 (2005).
- Mott, N. F. The basis of the electron theory of metals, with special reference to the transition metals. *Proc. Phys. Soc. Sect. A* **62**, 416–422 (1949).
- Lee, P. A., Nagaosa, N. & Wen, X.-G. Doping a Mott insulator: physics of high-temperature superconductivity. *Rev. Mod. Phys.* **78**, 17–85 (2006).
- Imada, M., Fujimori, A. & Tokura, Y. Metal-insulator transitions. *Rev. Mod. Phys.* **70**, 1039–1263 (1998).
- Salamon, M. B. & Jaime, M. The physics of manganites: structure and transport. *Rev. Mod. Phys.* **73**, 583–628 (2001).
- Murakami, Y., Golež, D., Eckstein, M. & Werner, P. Photo-induced nonequilibrium states in Mott insulators. Preprint at <https://doi.org/10.48550/arxiv.2310.05201> (2023).
- Stojchevska, L. et al. Ultrafast switching to a stable hidden quantum state in an electronic crystal. *Science* **344**, 177–180 (2014).
- Cavalleri, A. Photo-induced superconductivity. *Contemp. Phys.* **59**, 31–46 (2018).
- Najafi, E., Scarborough, T. D., Tang, J. & Zewail, A. Four-dimensional imaging of carrier interface dynamics in p-n junctions. *Science* **347**, 164–167 (2015).
- Liao, B., Najafi, E., Li, H., Minnich, A. J. & Zewail, A. H. Photo-excited hot carrier dynamics in hydrogenated amorphous silicon imaged by 4D electron microscopy. *Nat. Nanotechnol.* **12**, 871–876 (2017).
- Liao, B. & Najafi, E. Scanning ultrafast electron microscopy: a novel technique to probe photocarrier dynamics with high spatial and temporal resolutions. *Mater. Today Phys.* **2**, 46–53 (2017).
- Choudhry, U. et al. Persistent hot carrier diffusion in boron arsenide single crystals imaged by ultrafast electron microscopy. *Matter* <https://doi.org/10.1016/j.matt.2022.09.029> (2022).
- El-Zohry, A. M. et al. Extraordinary carrier diffusion on CdTe surfaces uncovered by 4D electron microscopy. *Chem.* **5**, 706–718 (2019).
- Wong, J. et al. Spatiotemporal imaging of thickness-induced band-bending junctions. *Nano Lett.* **21**, 5745–5753 (2021).
- Plumb, K. W. et al. α -RuCl₃: a spin-orbit assisted Mott insulator on a honeycomb lattice. *Phys. Rev. B* **90**, 041112 (2014).

16. Pollini, I. Electronic properties of the narrow-band material α -RuCl₃. *Phys. Rev. B* **53**, 12769–12776 (1996).
17. Kitaev, A. Anyons in an exactly solved model and beyond. *Ann. Phys.* **321**, 2–111 (2006).
18. Banerjee, A. et al. Neutron scattering in the proximate quantum spin liquid α -RuCl₃. *Science* **356**, 1055–1059 (2017).
19. Yokoi, T. et al. Half-integer quantized anomalous thermal Hall effect in the Kitaev material candidate α -RuCl₃. *Science* **373**, 568–572 (2021).
20. Do, S.-H. et al. Majorana fermions in the Kitaev quantum spin system α -RuCl₃. *Nat. Phys.* **13**, 1079–1084 (2017).
21. Tian, Y., Gao, W., Henriksen, E. A., Chelikowsky, J. R. & Yang, L. Optically driven magnetic phase transition of monolayer RuCl₃. *Nano Lett.* **19**, 7673–7680 (2019).
22. Boström, E. V., Sriram, A., Claassen, M. & Rubio, A. Controlling the magnetic state of the proximate quantum spin liquid α -RuCl₃ with an optical cavity. *npj Comput. Mater.* **9**, 202 (2023).
23. Zhang, J. et al. Ultrafast spin dynamics and photoinduced insulator-to-metal transition in α -RuCl₃. *Nano Lett.* <https://doi.org/10.1021/acs.nanolett.3c02668> (2023).
24. Sun, J., Melnikov, V. A., Khan, J. I. & Mohammed, O. F. Real-space imaging of carrier dynamics of materials surfaces by second-generation four-dimensional scanning ultrafast electron microscopy. *J. Phys. Chem. Lett.* **6**, 3884–3890 (2015).
25. Wang, Y. et al. Modulation doping via a two-dimensional atomic crystalline acceptor. *Nano Lett.* **20**, 8446–8452 (2020).
26. Najafi, E., Ivanov, V., Zewail, A. & Bernardi, M. Super-diffusion of excited carriers in semiconductors. *Nat. Commun.* **8**, 15177 (2017).
27. Strohmaier, N. et al. Observation of elastic doublon decay in the Fermi-Hubbard model. *Phys. Rev. Lett.* **104**, 080401 (2010).
28. Eckstein, M. & Werner, P. Thermalization of a pump-excited Mott insulator. *Phys. Rev. B* **84**, 035122 (2011).
29. Nevola, D. et al. Timescales of excited state relaxation in α -RuCl₃ observed by time-resolved two-photon photoemission spectroscopy. *Phys. Rev. B* **103**, 245105 (2021).
30. Kim, H.-S., Shankar, V. V., Catuneanu, A. & Kee, H.-Y. Kitaev magnetism in honeycomb RuCl₃ with intermediate spin-orbit coupling. *Phys. Rev. B* **91**, 241110 (2015).
31. Banerjee, A. et al. Proximate Kitaev quantum spin liquid behaviour in a honeycomb magnet. *Nat. Mater.* **15**, 733–740 (2016).
32. Eckstein, M. & Werner, P. Photoinduced states in a Mott insulator. *Phys. Rev. Lett.* **110**, 126401 (2012).
33. Shih, A., Yater, J., Hor, C. & Abrams, R. Secondary electron emission studies. *Appl. Surf. Sci.* **111**, 251–258 (1997).
34. Agapito, L. A., Curtarolo, S. & Nardelli, M. B. Reformulation of DFT+U as a pseudohybrid Hubbard density functional for accelerated materials discovery. *Phys. Rev. X* **5**, 011006 (2015).
35. Okamoto, H., Matsuzaki, H., Wakabayashi, T., Takahashi, Y. & Hasegawa, T. Photoinduced metallic state mediated by spin-charge separation in a one-dimensional organic Mott insulator. *Phys. Rev. Lett.* **98**, 037401 (2006).
36. Perfetti, L. et al. Femtosecond dynamics of electronic states in the Mott insulator 1T-TaS₂ by time resolved photoelectron spectroscopy. *N. J. Phys.* **10**, 053019 (2008).
37. Morrison, V. R. et al. A photoinduced metal-like phase of monoclinic VO₂ revealed by ultrafast electron diffraction. *Science* **346**, 445–448 (2014).
38. Yan, J.-Q. & McGuire, M. A. Self-selecting vapor growth of transition-metal-halide single crystals. *Phys. Rev. Mater.* **7**, 013401 (2023).
39. Andrade, X. et al. Real-space grids and the Octopus code as tools for the development of new simulation approaches for electronic systems. *Phys. Chem. Chem. Phys.* **17**, 31371–31396 (2015).
40. Tancogne-Dejean, N. et al. Octopus, a computational framework for exploring light-driven phenomena and quantum dynamics in extended and finite systems. *J. Chem. Phys.* **152**, 124119 (2020).
41. Tancogne-Dejean, N., Oliveira, M. J. T. & Rubio, A. Self-consistent DFT+U method for real-space time-dependent density functional theory calculations. *Phys. Rev. B* **96**, 245133 (2017).
42. Hartwigsen, C., Goedecker, S. & Hutter, J. Relativistic separable dual-space Gaussian pseudopotentials from H to Rn. *Phys. Rev. B* **58**, 3641–3662 (1998).

Acknowledgements

We thank Yuki Motome and Mengkun Liu for helpful discussions. This work is based on research supported by the US Air Force Office of Scientific Research under the award number FA9550-22-1-0468 (for the study of hot photocarrier dynamics) and by the US Army Research Office under the award number W911NF2310188 (for the development of SUEM). J.Y. was supported by the US Department of Energy, Office of Science, National Quantum Information Science Research Centers, Quantum Science Center (for sample growth).

Author contributions

Conceptualization: K.B., B.L.; Sample preparation: J.Y., K.H., E.L., K.B.; SUEM development: U.C., Y.Q., B.S., R.G.; SUEM measurement: U.C.; SUEM data analysis: U.C., B.L.; Theoretical analysis: J.Z., A.R.; Funding and project administration: K.B., B.L.; Supervision: A.R., K.B., B.L.; Writing – original draft: U.C., B.L.; Writing – review & editing: all authors.

Competing interests

The authors declare no competing interests.

Additional information

Supplementary information The online version contains supplementary material available at <https://doi.org/10.1038/s42005-025-02107-z>.

Correspondence and requests for materials should be addressed to Jin Zhang, Angel Rubio or Bolin Liao.

Peer review information *Communications Physics* thanks Spencer Reisbick and the other anonymous reviewer(s) for their contribution to the peer review of this work. A peer review file is available.

Reprints and permissions information is available at <http://www.nature.com/reprints>

Publisher's note Springer Nature remains neutral with regard to jurisdictional claims in published maps and institutional affiliations.

Open Access This article is licensed under a Creative Commons Attribution 4.0 International License, which permits use, sharing, adaptation, distribution and reproduction in any medium or format, as long as you give appropriate credit to the original author(s) and the source, provide a link to the Creative Commons licence, and indicate if changes were made. The images or other third party material in this article are included in the article's Creative Commons licence, unless indicated otherwise in a credit line to the material. If material is not included in the article's Creative Commons licence and your intended use is not permitted by statutory regulation or exceeds the permitted use, you will need to obtain permission directly from the copyright holder. To view a copy of this licence, visit <http://creativecommons.org/licenses/by/4.0/>.

© The Author(s) 2025